Nanoscale

PAPER

View Article Online
View Journal | View Issue

Cite this: *Nanoscale*, 2014, **6**, 842

Multi-walled carbon nanotube–graphene–polyaniline multiphase nanocomposite with superior electromagnetic shielding effectiveness†

Tejendra K. Gupta, Bhanu Pratap Singh, Rakesh B. Mathur and Sanjay R. Dhakate*

The multiphase approach was adapted to enhance the electromagnetic interference (EMI) shielding effectiveness (SE) of polyaniline (PANI) based nanocomposites. The natural graphite flakes (NGF) incorporated modified PANI was used for the development of multi-walled carbon nanotubes (MWCNTs) based nanocomposites. In PANINGF–MWCNTs composites, multilayer graphene was synthesized *in situ* by ball milling. The resultant PANINGF–MWCNTs nanocomposites were characterized by different techniques. It was revealed from the transmission electron microscope (TEM) observation that *in situ* derived multilayer graphene acts as a bridge between PANI and MWCNTs, and plays a significant role for improving the properties of multiphase nanocomposites. It was observed that EMI-SE increases with increasing the MWCNTs content from 1 to 10 wt% in the multiphase nanocomposites. The maximum value of total EMI-SE was −98 dB of nanocomposite with 10 wt% of MWCNTs content. The high value of EMI-SE is dominated by the absorption phenomenon which is due to the collective effect of increase in space charge polarization and decrease in carrier mobility. The decrease in carrier mobility has a positive effect on the shore hardness value due to the strong interaction between the reinforcing constituent in multiphase nanocomposites. As a consequence, shore hardness increases from 56 to 91 at 10 wt% of MWCNTs.

Received 27th August 2013
Accepted 11th October 2013

DOI: 10.1039/c3nr04565j

www.rsc.org/nanoscale

1. Introduction

Polymeric materials have been widely used in almost every sector of industry due to its unique properties. Among the different polymers, conducting organic polymers are a special class of material due to their interesting electrical and physical properties. These find potential applications in many areas such as energy storage devices and batteries,[1–3] electrochromic devices,[4] sensors,[5,6] anticorrosive materials,[7] electrostatic charge dissipation,[8] organic light emitting diode,[9,10] catalysis.[11] Due to their light weight, they may be used as electromagnetic interference (EMI) shielding materials[12] in many electronic devices.

Amongst conducting polymers, polyaniline (PANI) has become one of the most attractive polymers due to its high electric conductivity, lightness, environmental stability, and ease of synthesis.[12,13] However, the percolation threshold of PANI is high because of low compatibility and low aspect ratio of the conducting polymer.[14] The drawback of low electric conductivity and low specific strength restricts its application as EMI shielding material. To make it viable for commercial application, it required to disperse some requisite materials of micron or nanosize as reinforcement so it can be used in the form of composites for these applications. Many approaches have been undertaken to solve the problem of low electrical conductivity of PANI by inclusion of a conducting filler in the PANI matrix. During the past decade, improvements in EMI shielding effectiveness (SE) have been achieved by introducing carbon materials, such as carbon black, carbon fiber, exfoliated graphite, graphite, flyash, carbon nanotubes (CNTs) and even now multilayer graphene.[12,15–19]

To improve the properties of the PANI, Saini *et al.*[15] developed PANI based composite by *in situ* emulsion pathway technique with a different ratio of graphite and PANI. It is reported that by incorporating 15.6 wt% of graphite in PANI, the ultimate composite possesses electrical conductivity 12.5 S cm^{-1} and total EMI-SE is reached up to −33.6 dB in the X-band frequency region (8.2–12.4 GHz). In another course of investigation, Saini *et al.*[16] used colloidal graphite as reinforcement to improve the properties of PANI based composite, it is demonstrated that 17.4 wt% loading of colloidal graphite is able to enhance electrical conductivity up to 67.4 S cm^{-1} and EMI-SE upto −39.7 dB in the X-band frequency region. Singh *et al.*[17] incorporated 1 : 1 ratio of graphite oxide and Fe_3O_4 in the PANI matrix and achieved EMI-SE of −26 dB in Ku band region (12.4–18.0 GHz). The incorporation of fly ash in PANI in a ratio of 3 : 1 influences the

Physics & Engineering of Carbon, Division of Material Physics & Engineering, CSIR-National Physical Laboratory, Dr. K.S. Krishnan Road, New Delhi, 110012, India. E-mail: dhakate@mail.nplindia.org

† Electronic supplementary information (ESI) available. See DOI: 10.1039/c3nr04565j

EMI-SE of the composite and it increases to −32 dB in the X-band frequency range.[18] On the other hand, by addition of nanomaterials such as multi-walled carbon nanotubes (MWCNTs) in the PANI by *in situ* polymerization process, it was observed that at loading of 25 wt% MWCNT,[12] total EMI-SE of −39.2 dB was achieved in the Ku-band frequency range. Recently, Bingqing *et al.*[19] has developed a PANI based nanocomposite using single wall carbon nanotubes (SWCNTs) and graphene, and compared the EMI-SE of both nanocomposite. It is reported that addition of 25 wt% SWCNT and −33 wt% graphene sheets in the nanocomposite, gives a total EMI-SE of −31.5 dB and −34.2 dB, respectively.

So far, no attempt has been made to develop PANI based nanocomposite by using two types of reinforcing component *i.e.* micro- and nanophase, to improve electrical conductivity, EMI-SE and hardness. The primary objective of this work is to develop a PANI based nanocomposite with improved EMI-SE by a multi-scale approach. Pure PANI has very low electrical conductivity in the order of 1–2 S cm^{-1}. Therefore, initially PANI is modified by incorporation of a few weight percentages of natural graphite flakes (NGF) to improve the electrical conductivity of PANI. Later on, modified PANI based nanocomposites are developed with inclusion of different weight fractions of MWCNTs. The mixture of modified PANI and MWCNTs was ball milled for several hours to generate *in situ* graphene in the nanocomposites. To ascertain a multi-scale approach on the properties of PANINGF–MWCNTs nanocomposites, these were characterized by SEM, TEM, Raman spectroscopy, X-ray diffraction and vector network analyzer (VNA) for EMI-SE.

2. Experimental and characterization

2.1. Materials

MWCNTs were synthesized by a catalytic chemical vapor deposition (CVD) technique in the laboratory[20,21] and used in this investigation. As-produced MWCNTs are less reactive and as a result make poor bonding with a matrix or other additives. To improve the bonding of MWCNTs with other reinforcing constituents, these MWCNTs were functionalized by an oxidation reaction with concentrated nitric acid.[22–24]

2.2. Polyaniline–natural graphite flakes

PANI was synthesized and modified by *in situ* chemical oxidative polymerization[16] of aniline (AN) in the presence of dispersed NGF particles and supplied by a conducting polymer section of NPL. The precipitate obtained was dried in a vacuum oven at 60 °C and abbreviated as PANINGF.

2.3. Fabrication of nanocomposites

The PANINGF and MWCNT–PANINGF composite were fabricated by solvent mixing followed by high speed homogenization and a ball milling technique for 20 h. Initially PANINGF were dissolved in toluene using magnetic stirring for 6 h and acid modified MWCNTs were dispersed in toluene for 6 h using ultrasonication. The dispersed MWCNTs and dissolved PANINGF were mixed thoroughly using high speed homogenization for 30 min and the mixed solution was dried in a vacuum oven at 80 °C for 12 h to evaporate the solvent. The dried powder mixture was then mixed again using ball milling for 20 h at a rate of 300 rpm and the composites were fabricated by a compression molding technique using three piece die mold (size 60 × 20 × 2.5 mm). This process was repeated for 0, 1.0, 5.0, 7.0 and 10.0 wt% of MWCNT loading and designated as PCNT0, PCNT1, PCNT5, PCNT7 and PCNT10, respectively.

2.4. Characterization

The surface morphology of the as-produced MWCNTs, functionalized MWCNTs and PANI based nanocomposites was observed by SEM (Leo model: S-440). The detailed morphology of MWCNTs and PANINGF–MWCNTs was also observed by transmission electron microscopy (TEM) using Technai G20, 300 kV FEG.

Raman spectra of the samples were recorded using Renishaw inVia Raman Spectrometer, UK with a laser as an excitation source at 514 nm. The electrical conductivity of the composite films (60 × 20 × 2 mm) was measured by d.c. four probe contact method[25–27] using a Keithley 224 programmable current source for providing current. The voltage drop was measured on a Keithley 197A auto ranging digital microvoltmeter. The values reported in the text are averaged over six readings of voltage drops at different portions of the sample.

EMI-SE was measured by a waveguide using VNA (E8263BAgilent Technologies). The rectangular samples of thickness 2.50 mm were placed inside the cavity of the sample holder which matches the internal dimensions of the Ku-band (12.4–18 GHz) wave guide. The sample holder was placed between the flanges of the waveguide connected between the two ports of VNA. A full two port calibration was performed using a quarter wavelength offset and terminations and keeping input power level at −5.0 dBm. The shore hardness of the multiphase nanocomposite was measured using a shore hardness instrument made by Coats Machine Tool Co. Ltd, London.

3. Results and discussion

3.1. Characteristics of MWCNTs

The MWCNTs are synthesized by CVD technique in the laboratory using the organometallic compound ferrocene as catalyst and toluene as carbon source. Fig. 1(a) shows a SEM image of as-produced long and aligned MWCNTs entangled with each other due to weak van der Waal interactions between them. The diameter of the tubes is in the range 10–70 nm and average bundle length of ∼300 μm,[22] in which there is no evidence of amorphous carbon particles. In Fig. 1(b), a SEM micrograph of functionalized MWCNTs is distinct from the SEM micrograph of as-produced MWCNTs, in which the end of the tubes is exfoliated (insert in Fig. 1(b)) due to oxidation of nanotube caps (pentagon–heptagon pair defects). These functionalized MWCNTs are more reactive due to the presence of dangling bonds. To understand the surface morphology of MWCNTs in detail, it is characterized using TEM. It is observed that the

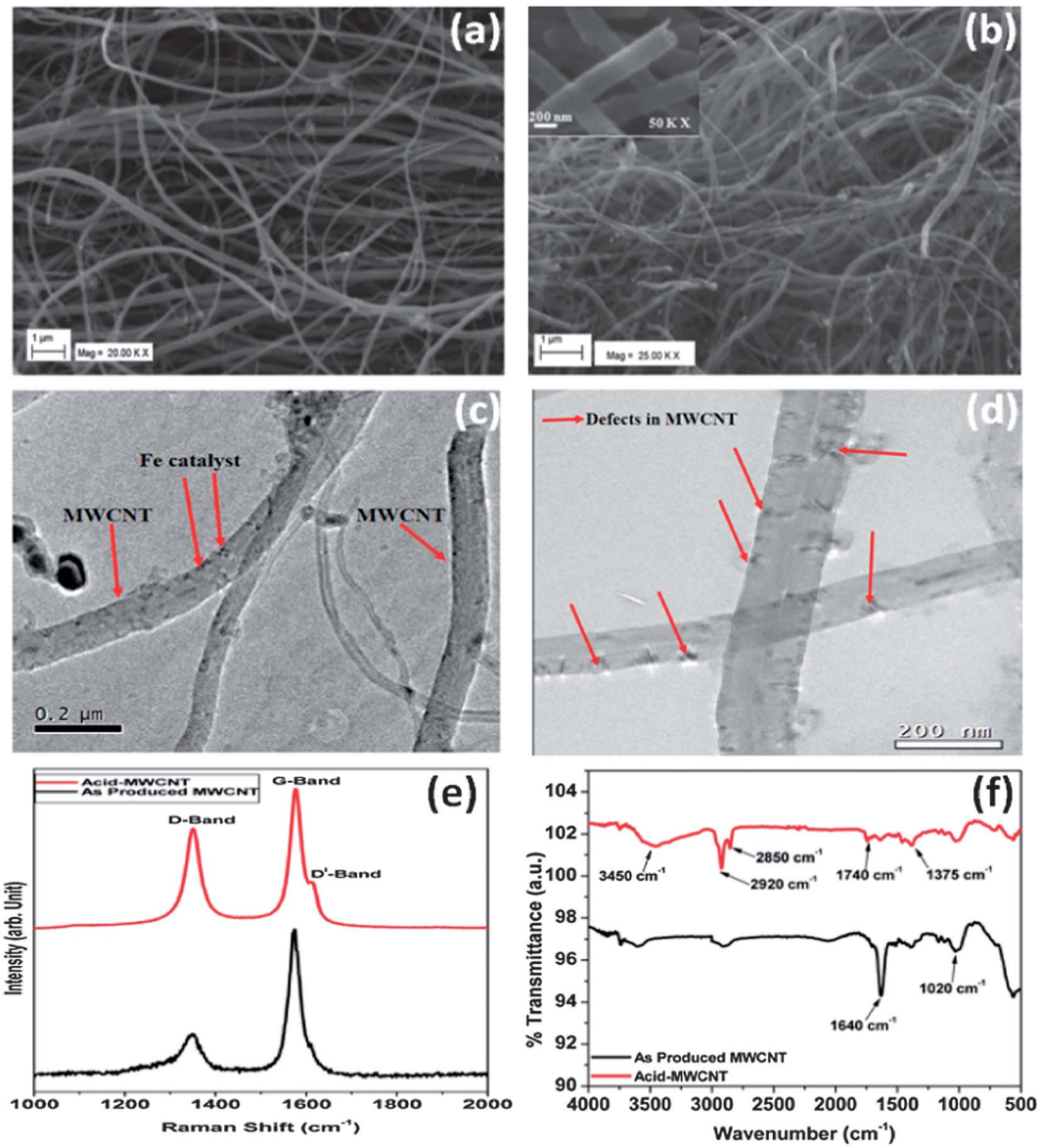

Fig. 1 SEM (a and b), TEM (c and d) images, Raman spectra (e) and FTIR (f) spectra of as-produced and acid functionalized MWCNTs.

surface of the as-produced MWCNTs is smooth and the iron catalyst particles are encapsulated in it, which is visible in the form of a black spot (Fig. 1(c)). Fig. 1(d) shows a TEM image of acid functionalized MWCNTs in which the surface pits in the form of defects generated due to oxidation by concentrated acid treatment. However, there is no evidence of iron catalyst particles which might be dissolved during the acid treatment and washed out in the processing.

Fig. 1(e) shows a comparison of Raman spectra of as-produced and acid functionalized MWCNTs on the basis of I_G/I_D ratio. Three distinct peaks are shown in the spectra in which the first peak is for D band, induced by the structural disorder of the tubes located at 1346 and 1352 cm^{-1} for as-produced and acid functionalized MWCNTs, respectively. The second peak is for G band which is associated with the tangential stretching mode of the graphitic C=C bond and is located at 1580 and 1576 cm^{-1} for as-produce and acid functionalized MWCNTs, respectively. The third peak comes into view as a shoulder of the G-band at higher frequency and was observed at 1612 and 1615 cm^{-1} for as-produced and acid functionalized MWCNTs, respectively, and is designated as the D′ band. D′ band is similar to the D band and originates from a double resonance Raman process induced by structural disorder. Thus, the intensity of the D band (I_D) is associated with the presence of defects in the nanotubes, while the intensity of G band (I_G) is independent of the structural disorder. From the figure, a major change in the I_G/I_D ratio is observed in the Raman spectra and it was found that the I_G/I_D for as-produced MWCNTs is 2.78 and 1.29 for acid functionalized MWCNTs. The significant drop off in the I_G/I_D ratio further confirms addition of functional groups in the form of defects which are generated during acid treatment. These defects are verified by characterizing of as grown and

functionalized MWCNTs using FTIR. Fig. 1(f) shows FTIR spectra of as grown and functionalized MWCNTs. The FTIR spectra of as grown MWCNTs display peaks at 1640 and 1020 cm^{-1} which are due to C=C bond and C–C bond, respectively, which form the framework of the CNT sidewall.

However, after oxidation some new peaks are introduced due to functionalization of MWCNTs. The peak at 1740 cm^{-1} is associated with the stretching mode of carboxylic groups (–C=O) attached to MWCNTs. The broad peak at 3450 cm^{-1} can be assigned to the O–H stretching vibrations of carboxylic groups (O=C–OH). These two peaks are an indication of acid functionalization. While the peak at 2920 cm^{-1} for $-CH_2$ antisymmetric stretching, 2850 cm^{-1} for $-CH_3$ symmetric stretching and 1375 cm^{-1} for $-CH_3$ symmetric bending vibrations, respectively which are produced at the defect sites of acid-oxidized MWCNT surface. These observations are in good agreement with the results of SEM, TEM and Raman spectroscopy data of functionalized MWCNTs.

Fig. 2 shows a schematic of the processing of PANINGF and PANINGF–MWCNTs nanocomposites. The PANI was initially modified by incorporating 5 wt% NGF to produce PANINGF by *in situ* chemical oxidative polymerization.[16] The NGF has a layered structure in which the individual graphene sheets are separated by 0.3345 nm. Therefore, there is possibility of absorption of aniline molecules on the surface of the flakes and in the interlayers spacing. The absorption of aniline in the interlayer spacing possibly exfoliates the NGF. The mixing is carried out by ball milling which can also be used for the preparation of graphene sheets due to a mechanical and shear force acting on the NGF.[28] The PANINGF is mixed with different content (0, 1.0, 5.0, 7.0 and 10.0 wt fraction) of functionalized MWCNTs and then ball milled for 20 h. The ball milling is carried out in the a planetary ball mill in moist environment. In the NGF, each graphene layer is bonded with weak van der Waal forces and due to a shear force applied by milling impact, the NGF is exfoliated into graphene sheets. The continuous ball milling of PANINGF and MWCNTs can result in decreases in the grain size of the graphene layers as well as a change in the morphology of MWCNTs.

Fig. 3(a) shows a TEM micrograph of the PANINGF mixture. It shows that NGF is encapsulated in PANI and the aniline molecule is attached to NGF due to oxidative polymerization (shown by dashed circles). However, in Fig. 3(b), the TEM image of PANINGF–MWCNTs after milling in the planetary ball mill shows that the NGF is converted to the multilayer semi-transparent graphene sheets (shown by dashed circles) and is well bonded to MWCNTs and PANI (indicated by arrows). The graphene layers formed which are not of a uniform size and numbers of layers are varying throughout the material. This is validated by the TEM image in which graphene shows different reflections within Fig. 3(b) and as a consequence of the variation in the number of graphene layers. The interconnection between the graphene layers and MWCNTs can be a better pathway for improving the properties of nanocomposites.

3.2. Electrical conductivity of nanocomposites

Fig. 4 shows variation in the electrical conductivity of PANINGF–MWCNTs nanocomposites with increasing MWCNTs content. It is well known that even though the PANI is a class of conducting polymers, its electrical conductivity is not comparable to that of MWCNTs and graphene. However inclusion of multilayer graphene and MWCNTs significantly influences the electrical conductivity of PANI. It is reported in earlier reports that the electrical conductivity of PANI is in the order of 1–2 S

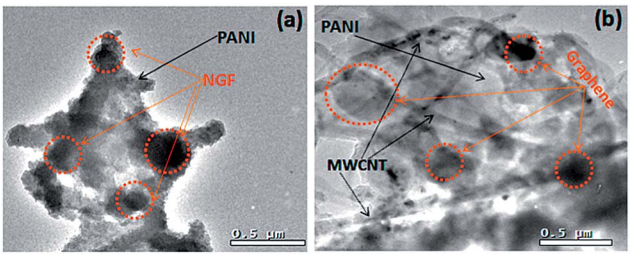

Fig. 3 TEM image of (a) PANINGF and (b) PANINGF–MWCNTs.

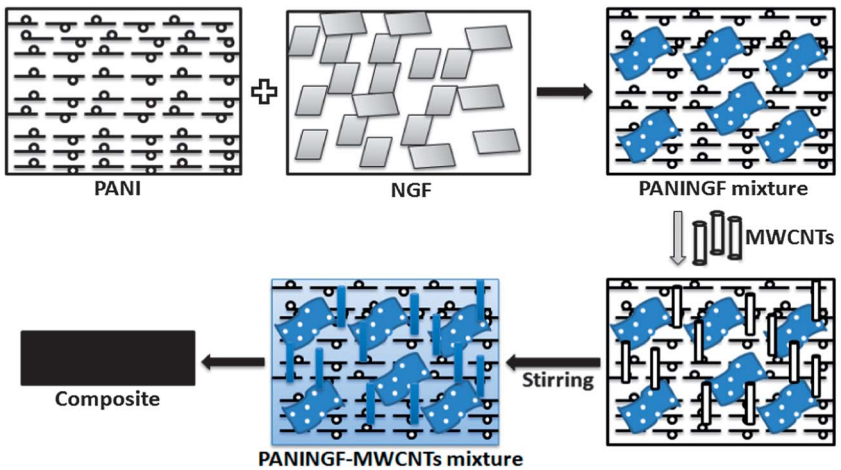

Fig. 2 Schematic of the processing of PANINGF and PANINGF–MWCNTs nanocomposites.

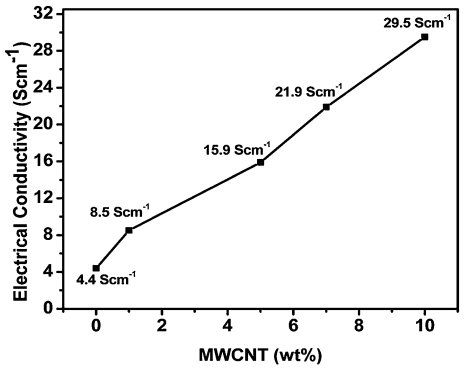

Fig. 4 Electrical conductivity of PANINGF composites with different MWCNTs loadings.

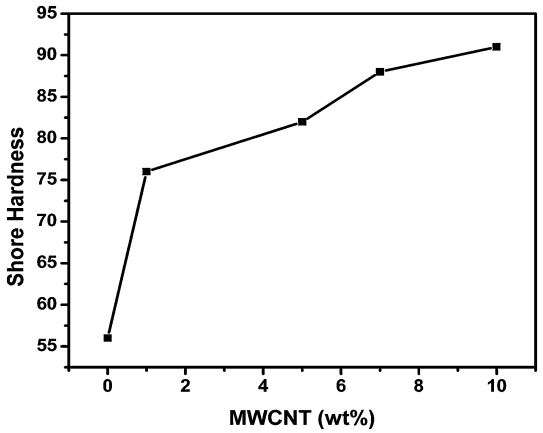

Fig. 5 Shore hardness of multiphase composites with different MWCNTs loadings.

cm^{-1}, while by incorporation of NGF in PANI during the processing, the electrical conductivity of PANI increases fourfold, which is attributed to the development of a conductive network. However, after reinforcing a different weight fraction of MWCNTs in the PANINGF, the electrical conductivity of the nanocomposite increases continuously. The extent of increase in the electrical conductivity is directly proportional to the increase in the MWCNTs content in the nanocomposites. For nanocomposites with 1 wt% of MWCNTs (PCNT1), electrical conductivity is 8.5 S cm^{-1} and with increasing MWCNTs content up to 10 wt%, electrical conductivity increases from 8.5 to 15.9, 15.9 to 21.9 and 21.9 to 29.5 S cm^{-1} for PCNT5, PCNT7 and PCNT10, respectively. This depends on the conductive network formation by MWCNTs and graphene in the polymer matrix. These observations are confirmed from the SEM micrographs of the nanocomposites shown in Fig. 6 and the TEM image in Fig. 3(b).

3.3. Shore hardness of nanocomposites

Hardness is a measure of the material resistance to various kinds of permanent shape changes when a force is applied. The shore hardness of pure PANI is very low according to the literature. In this study, initially, PANI is modified by incorporating multilayer graphene sheets generated by ball milling of NGF and the shore hardness of PANINGF and MWCNTs incorporated PANINGF multiscale composites is measured by a scleroscopic hardness tester. The scleroscopic hardness is also known as dynamic hardness which measures the height of the bounce of a diamond tipped hammer dropped from a fixed height on the materials. This type of hardness is related to elasticity. Generally the polymer materials have very low hardness but with inclusion of other micro- or nanofiller, the value of the hardness improves remarkably, even though the graphite possesses poor shore hardness due to the soft and brittle nature of material. On the other hand, in the case of graphene, the carbon atoms bonded strongly with the covalent type of bonding that possesses a much higher value of hardness. Therefore, modified PANI has a shore hardness in the range of 50–56 which is much higher than the value of PANI (Fig. 5). On the other hand, the value of the multiscale nanocomposites, with increasing the functionalized MWCNTs, value of shore hardness increases continuously. It increases from 56 for PCNT0 to 91 for PCNT10; this is attributed to the strong interaction between the modified PANI and functionalized MWCNTs.

Fig. 6 shows SEM micrographs of PANINGF–MWCNTs nanocomposites with different weight fractions of MWCNTs loading. In the case of 1 wt% MWCNTs incorporated PANINGF nanocomposite (PCNT1), MWCNTs are not separately visible, encapsulated in between the PANI and graphene sheets (Fig. 6(a)). With increasing the MWCNTs concentration in the nanocomposites the extent of visibility of the nanotubes increases, but still most of the nanotubes are of different lengths and encapsulated in the polymer matrix. This is evidence that the mechanical and shear force acting during ball milling of the mixture can reduce the size of the constituents in the nanocomposites (Fig. 6 (b) & (c)).

Also, in the case of PCNT10, some graphene sheets are visible along with MWCNTs (Fig. 6c). Even at 10 wt% of MWCNTs, there is formation of MWCNTs interface in the multiphase nanocomposites to some extent (visible in Fig. 6(c)).

Raman spectroscopy is one of the most useful characterization techniques for carbon materials[29] and carbon material incorporated composites.[22] In the case of graphite, it has three most intense Raman features at ~1580 cm^{-1} (G band), ~1350 cm^{-1} (D band) and ~2700 cm^{-1} (2D band). Fig. 7 shows the Raman spectra of multilayer graphene incorporated PANI and its composite with inclusion of MWCNTs. Fig. 7(a) shows the Raman spectra of PANI with *in situ* generated multilayer graphene in it. Generally, the sharp single peak at around 2700 cm^{-1} (2D region) represents single layer graphene, while in-between 2600 and 2700 cm^{-1} a modulated bump is present for multilayer graphene generated during ball milling of PANINGF. The presence of a modulated bump at 2700 cm^{-1} is clear evidence of the presence of multilayer graphene and this is confirmed by a comparison of the Raman spectra of multilayer graphene and graphite shown in the ESI† (Fig. S1). Fig. 7(b) shows the Raman spectra of PANINGF–MWCNTs composites. In PANINGF and PANINGF–MWCNTs composites, C–H bending

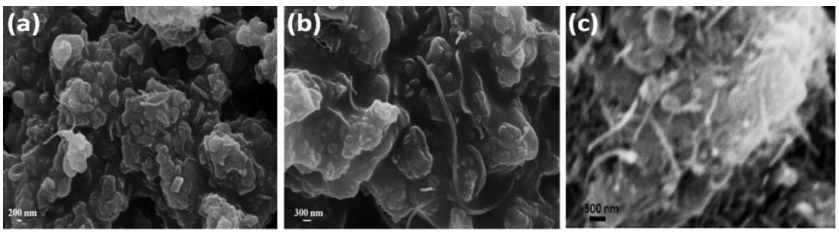

Fig. 6 SEM micrographs of nanocomposites with different weight percentages of MWCNTs (a) PCNT1, (b) PCNT5 and (c) PCNT10.

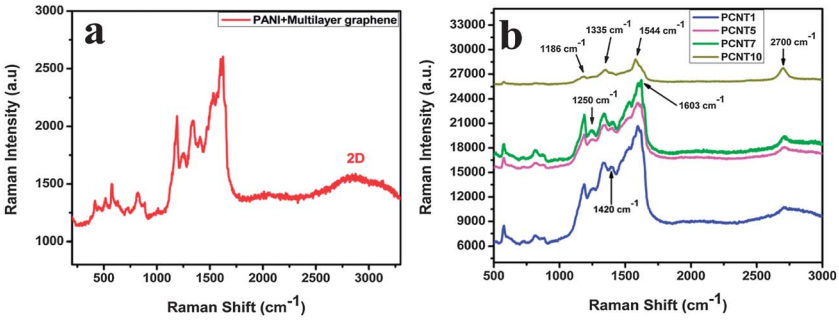

Fig. 7 Raman spectra of (a) PANINGF and (b) PANINGF–MWCNT composites at different MWCNT loadings.

of the quinoid ring at 1186 cm^{-1}, C–H bending of the benzenoid ring at 1250 cm^{-1}, C–N^{+} stretching at 1335 cm^{-1}, and C–C stretching of the benzene ring at 1420 and 1603 cm^{-1} are observed which reveals the presence of doped PANI structures.[30] This clearly suggests that Raman spectra are almost identical to those of PANINGF and PANINGF–MWCNTs composites, indicating that MWCNT serves as the core in the formation of a tubular shell of PANINGF–MWCNTs composites *i.e.* MWCNTs are encapsulated in the PANINGF matrix. These observations are in good agreement with SEM studies. The peaks at 1580 and 2700 cm^{-1} show presence of G-band and second order defects due to the carbon nanostructure (multilayer graphene and CNTs) in the PANI composites. However, with increasing the MWCNTs content the peaks intensity of PANI decreases.

3.4. Electromagnetic shielding measurements

EMI-SE is defined as the attenuation of the propagating electromagnetic (EM) waves produced by the shielding material. EMI shielding refers to the reflection and absorption of electromagnetic radiation by the material.[25,31,32] In the case of reflection of the radiation by the shielding material, the shield material must have a mobile charge carrier (electron or holes) which interacts with the electromagnetic field in the radiation. As a result, the shield material tends to be electrically conducting. However, the absorption of shield material depends on the electric or magnetic dipoles which interact with the electromagnetic field of the radiation. Other than reflection and absorption, a mechanism of shielding is multiple reflections, which refer to the reflection at different surfaces or interfaces in the shield material. This mechanism requires the presence of a large surface area or interface area in the shield material. The losses due to multiple reflections can be ignored when the distance between the reflecting surface and interface is large, compared to the skin depth.

The electromagnetic radiations at high frequencies penetrate only near the surface region of the conducting material and this phenomenon is known as skin effect.[22,33,34] In this study, PANI is modified by incorporating 5 wt% of NGF, later on is converted to multilayer graphene. It is used to make nanocomposites with different weight fractions of functionalized MWCNTs. EMI-SE measurements of these multiphase nanocomposites are carried out in the Ku-band (12.4–18.0 GHz). When electromagnetic radiation is incident on the material, the sum of absorption (A), reflection (R) and transmission (T) must be the value "one", that is, $T + R + A = 1$.

Fig. 8 shows the variation in EMI-SE of a multiscale nanocomposite with increasing MWCNTs content. Fig. 8(a) shows the shielding effectiveness due to absorption (SE_A) with increasing the MWCNTs content in the nanocomposites. It is observed that SE_A of electromagnetic radiation continuously increases with increasing the MWCNTs content while it is almost constant with increasing the frequency from 12.4 to 18 GHz.

In the same pattern the shielding effectiveness due to reflection (SE_R) increases with increasing the MWCNTs content (Fig. 8(b)) and the resultant value is one order of magnitude less than SE_A, even though electrical conductivity increases with increasing MWCNTs content. Fig. 8(c) shows that the total shielding effectiveness (SE_T) increases with increasing MWCNTs content. At 0 wt% of MWCNTs loading (PCNT0), SE_T is reached a very high value of −46 dB which is due to the multilayer graphene incorporated in PANI. However, the SE_T value for PCNT1, PCNT5, PCNT7 and PCNT10 is found to be −48, −69, −78 and −98 dB, respectively. The extent of increase in SE_T corresponds to the extent of MWCNTs incorporated in

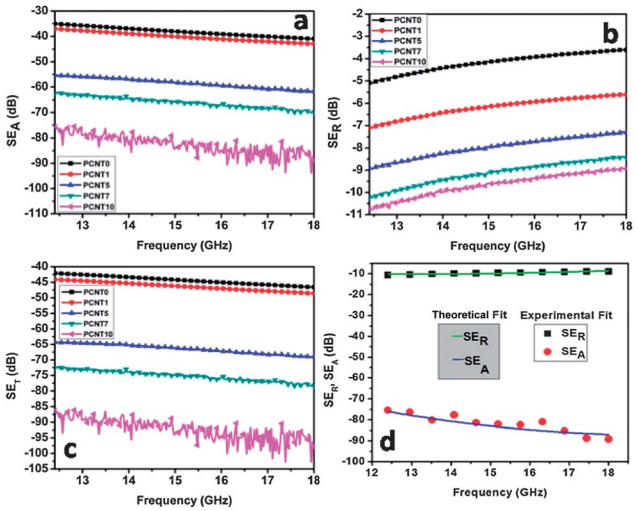

Fig. 8 Dependence of shielding effectiveness due to (a) absorption (SE_A), (b) reflection (SE_R), (c) total (SE_T) of composites on frequency and (d) comparison of theoretical and experimental shielding effectiveness (SE_R and SE_A) for the composites with respect to frequency.

PANINGF multiscale nanocomposite. This value of SE_T is dominated by the absorption phenomena as compared to the reflection. It is well known that the SE_T of PANI is dominated by absorption phenomena due to the presence of localized charges (polarons and bipolarons) leading to strong divergence and relaxation effect.[17,18] Even though in the multiscale nanocomposite, with addition of MWCNTs, the skin depth deceases, the coating of PANI on the MWCNTs can dominate the polarization and the functional groups of functionalized MWCNTs results into the absorption of electromagnetic radiation.[22] It is well known that the functional groups of nanotubes are also responsible for the absorption, as increasing the content of MWCNTs functional groups which are responsible for the absorption of electromagnetic radiation increases. Fig. 8(d) compares the experimental and theoretical values of SE_R and SE_A with increasing the frequency. It is found that both theoretical and experimental results are in good agreement with each other.

Fig. 9(a) illustrates the variation of EMI-SE with MWCNT loading and the inset figure of Fig. 9(a) shows the values of SE with respect to electrical conductivity. Enhanced absorption can be explained in terms of reduction of the skin depth with the increase in the content of functionalized MWCNTs. The above results predict that shallow skin depths make it possible to achieve the same level of attenuation with a thinner shield of the same material. In other words, at the same thickness, the material with shallowest skin depth is expected to give the maximum absorption loss.[35] The variation of skin depth is shown in Fig. 9(b) with respect to wt% of MWCNT and the inset figure of Fig. 9(b) shows the variation of skin depth with respect to the frequency of different loadings of MWCNT in multiphase nanocomposites. The results demonstrate that skin depth decreases with increases in the frequency, which is responsible for the enhancement of absorption loss with frequency. Thus, for a given thickness, the absorption loss increases with decrease in skin depth *i.e.* from PCNT0 to PCNT10.

The total EMI-SE is dominated by the absorption of electromagnetic radiation. However, the absorption of shield material depends on the electric or magnetic dipoles which interact with the electromagnetic field of the radiation. Therefore, understanding of other attributes of the shield *i.e.* dielectric constant and dielectric loss is required. The parameter ε' represents the charge storage (dielectric constant) while ε'' is a measure of dielectric loss. The *in situ* incorporation of multilayer graphene during the ball milling in air environment generates mostly defective graphene (ESI-1†) which consists of a functional group attached on the graphene sheets. This further enhancs the strong polarization effects in modified PANI. On the other hand, in the case of PANINGF–MWCNTs multiscale nanocomposites, with increasing the concentration of functionalized MWCNTs in the modified PANI induced the confined charges; this results in increasing the dielectric constant and dielectric loss, which is demonstrated in Fig. 10. Fig. 10(a) shows that the dielectric constant (ε') is only 2.3 for PCNT0 but increases from 29 to 168 for PCNT1 to PCNT10, respectively at 18.0 GHz frequency. Similarly, the loss factor (ε'') is only 1.90 for PCNT0 but increases from 52 to 206 for PCNT1 to PCNT10, respectively at 18.0 GHz frequency (Fig. 10(b)).

The increase in dielectric constant and dielectric loss are due to the space charge establishment due to the significant difference between the electrical conductivity value of MWCNTs and the low conducting PANI matrix which donates toward interfacial polarization. However, the dielectric constant and

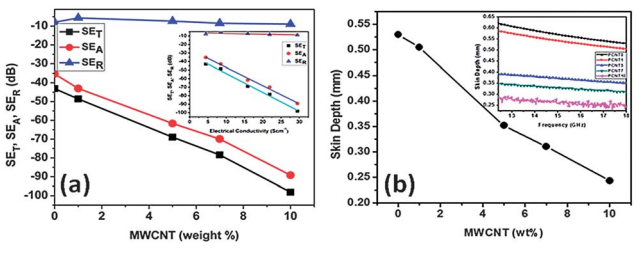

Fig. 9 (a) Effect of MWCNT loading of PANINGF–MWCNT composites on SE_T, SE_A and SE_R, inset figure shows the variation of shielding effectiveness (SE_T, SE_A and SE_R) for the composites with respect to electrical conductivity and (b) skin depth with respect to MWCNT wt%, inset figure shows the skin depth with respect to frequency.

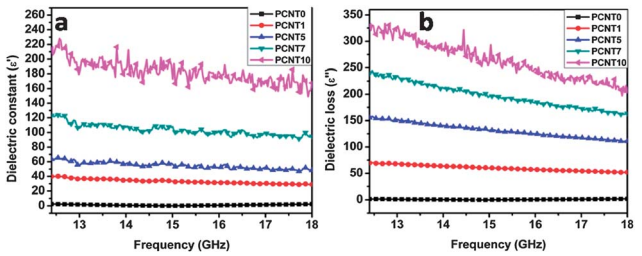

Fig. 10 Frequency dependence of the electromagnetic attributes of the multiphase nanocomposite: (a) dielectric constant (ε') and (b) dielectric loss (ε''').

Table 1 Electromagnetic shielding properties of different PANI based composites

Types of filler material	Filler wt%	Electrical conductivity (S cm^{-1})	Frequency range (GHz)	Shielding effectiveness (dB)	Ref.
Camphor sulfonic acid	—	—	0.1–1000 MHz	−39	Mäkelä *et al.*[36]
MWCNT	10	33.374	—	—	Zengin *et al.*[37]
PANI in PU	16	22	8.2–18 GHz	−40	Hoang *et al.*[38]
TiO_2	—	—	10–13 GHz	−31	Phang *et al.*[39]
Carbo black	30	0.8452	2–18 GHz	−40	Wu *et al.*[40]
Graphite	15.6	12.5	8.2–12.4 GHz	−33.6	Saini *et al.*[15]
Colloidal graphite	17.4	67.4	8.2–12.4 GHz	−39.7	Saini *et al.*[16]
MWCNT	25	19.7	12.4–18 GHz	−39.2	Saini *et al.*[12]
$BaFe_{12}O_{19}$	—	—	2–18 GHz	−13	Ting *et al.*[41]
CoTi doped $BaFe_{12}O_{19}$	—	—	2–18 GHz	−45.2	Du *et al.*[42]
γ-MnO_2	—	9.78×10^{-4}	2–18 GHz	−21	Jianjun *et al.*[43]
Oxyfluorinated MWCNT	—	14.6	800 MHz to 2.5 GHz	−47.03	Yun *et al.*[44]
SWCNTs/GNS	1	16.2	—	−27.0	Chen *et al.*[45]
MWCNT	30	0.035	12.4–18 GHz	−45.7	Saini *et al.*[46]
SWCNT	25	10	2.0–18 GHz	−31.5	Bingqing *et al.*[19]
Graphene	33	19	2.0–18 GHz	−34.2	Bingqing *et al.*[19]
EG–cobalt ferrite	1	86.207	2–18 GHz	−19.13	Chen *et al.*[47]
Graphene	—	—	2–18 GHz	−45.1	Yu *et al.*[48]
Fe_3O_4–MWCNT	20	—	2–18 GHz	−16.0	Cao *et al.*[49]
Gold nanoparticles and RGO	—	8.65	1–12 GHz	−108	Basavaraja *et al.*[50]
PANI : Fe_3O_4	15 : 10	—	12.4–18 GHz	−42	Belaabed *et al.*[51]
Sb_2O_3	50	—	8.2–12.4 GHz	−21	Faisal *et al.*[52]
Silicon carbide	—		26.5–40 GHz	−36.3	Li *et al.*[53]
para-Toluidine sulfonic acid (PTSA)–FeNi		10^{-2}	9.52 GHz	−22	Kamchi *et al.*[54]
$CuCl_2$	4	2.63×10^{-7}	8.2–12.4 GHz	−46.54	Bhattacharya *et al.*[55]
Graphene and MWCNTs	5 : 10	29.5	12.4–18 GHz	−98	Present work

dielectric losses slightly decrease with increasing the frequency in the composites but there is no significant decrease with increasing the content of MWCNTs in the nanocomposite at any fixed frequency. The composite with 10 wt% of MWCNTs loading (PCNT10) shows a very superior value of both the dielectric constant ($\varepsilon' = 168$) and dielectric loss ($\varepsilon''' = 206$). This is due to increase in space charge polarization and decrease in carrier mobility. The collective effect of space and charge polarization is responsible for the high value of the dielectric constant and dielectric losses. This attributes to SE dominated by the absorption phenomena.

Table 1 compares the electromagnetic shielding properties of different PANI based composites reported in the literature. The SE value of ~98 dB of multiphase nanocomposites in the present work is the second highest among the reported values of SE in the open literature. The highest value reported is of gold nanoparticles-reduced graphene oxide composites. However for the commercial applications, the gold nanoparticle based composites are not a viable and cost effective technology.

4. Conclusions

The multiphase nanocomposite of PANINGF–MWCNTs was fabricated by solvent mixing followed by high speed homogenization and a ball milling technique. The ball milling of PANINGF results in multilayer graphene in the nanocomposite. The presence of multilayer graphene in the PANI has a significant role for improving the properties. The electrical conductivity and shore hardness of the nanocomposite increase with increasing the functionalized MWCNTs content. The maximum value of shore hardness and EMI-SE is 91 and 98 dB for 10 wt% of MWCNTs in the nanocomposites. The extent of the increase in electrical conductivity is not as expected as a result of degradation in the properties of MWCNTs due to chemical functionalization but on the other hand that helps in improving the EMI-SE dominated by the absorption phenomena. However, the shielding effectiveness increases with MWCNTs content in the PANINGF–MWCNTs composites. The improvement of the EMI-SE is due to the synergetic effect of functionalized MWCNTs and *in situ* generated multilayer graphene and oxidative polymerized PANI. This can attribute to the collective effect of increasing in space charge polarization and decreasing in carrier mobility. The decrease in carrier mobility due to a strong interaction between the reinforcing constituent has a positive effect on the shore hardness of multiphase nanocomposites and the maximum value of shore hardness is 91 at 10 wt% of MWCNTs.

Acknowledgements

The authors are very grateful to the Director of CSIR-NPL for his kind permission to publish the results. The authors are thankful to the Polymeric & Soft Materials Section for providing modified PANI and measurement of EMI shielding. We are also thankful to Dr Vidyanand Singh for TEM measurement and also

to Mr Jai Tawale, Mr K.N. Sood for carrying out SEM at NPL. One of the authors (Tejendara Gupta) would like to thank CSIR for SRF fellowship.

References

1 A. Mohammadi, O. Inganäs and I. Lundström, *J. Electrochem. Soc.*, 1986, **133**, 947–949.
2 P. Novák, K. Müller, K. S. V. Santhanam and O. Haas, *Chem. Rev.*, 1997, **97**, 207–282.
3 T. Osaka, K. Naoi and S. Ogano, *J. Electrochem. Soc.*, 1988, **135**, 1071–1077.
4 H. Yashima, M. Kobayashi, K. B. Lee, D. Chung, A. J. Heeger and F. Wudl, *J. Electrochem. Soc.*, 1987, **134**, 46–52.
5 P. N. Bartlett and R. G. Whitaker, *J. Electroanal. Chem.*, 1987, **224**, 27–35.
6 C. Dhand, S. K. Arya, S. P. Singh, B. P. Singh, M. Datta and B. D. Malhotra, *Carbon*, 2008, **46**, 1727–1735.
7 M. Ioniţă and A. Prună, *Prog. Org. Coat.*, 2011, **72**, 647–652.
8 J.-Y. Kwon and H.-D. Kim, *J. Appl. Polym. Sci.*, 2005, **96**, 595–604.
9 H. S. Woo, R. Czerw, S. Webster, D. L. Carroll, J. Ballato, A. E. Strevens, D. Obrien and W. J. Blau, *Appl. Phys. Lett.*, 2000, **77**, 1393–1395.
10 P. Fournet, J. N. Coleman, B. Lahr, A. Drury, W. J. Blau, D. F. O'Brien and H. H. Horhold, *J. Appl. Phys.*, 2001, **90**, 969–975.
11 X. Gong, J. Liu, S. Baskaran, R. D. Voise and J. S. Young, *Chem. Mater.*, 2000, **12**, 1049–1052.
12 P. Saini, V. Choudhary, B. P. Singh, R. B. Mathur and S. K. Dhawan, *Mater. Chem. Phys.*, 2009, **113**, 919–926.
13 J. Joo and C. Y. Lee, *J. Appl. Phys.*, 2000, **88**, 513–518.
14 M. J. R. Cardoso, M. F. S. Lima and D. M. Lenz, *Materials Research*, 2007, **10**, 425–429.
15 P. Saini, V. Choudhary, K. N. Sood and S. K. Dhawan, *J. Appl. Polym. Sci.*, 2009, **113**, 3146–3155.
16 P. Saini, V. Choudhary and S. K. Dhawan, *Polym. Adv. Technol.*, 2009, **20**, 355–361.
17 K. Singh, A. Ohlan, V. H. Pham, B. R. S. Varshney, J. Jang, S. H. Hur, W. M. Choi, M. Kumar, S. K. Dhawan, B.-S. Kong and J. S. Chung, *Nanoscale*, 2013, **5**, 2411–2420.
18 A. K. Singh, A. P. Singh, A. Chandra and S. K. Dhawan, *AIP Adv.*, 2011, **1**, 022147.
19 Y. Bingqing, Y. Liming, S. Leimei, A. Kang and Z. Xinluo, *J. Phys. D: Appl. Phys.*, 2012, **45**, 235108.
20 R. B. Mathur, S. Chatterjee and B. P. Singh, *Compos. Sci. Technol.*, 2008, **68**, 1608–1615.
21 V. Choudhary, B. P. Singh and R. B. Mathur, Carbon Nanotubes and Their Composites, in *Carbon Nanotubes and Their Composites, Syntheses and Applications of Carbon Nanotubes and Their Composites*, ed. Dr S. Suzuki, ISBN: 978-953-51-1125-2, InTech, 2013, DOI: 10.5772/52897.
22 T. K. Gupta, B. P. Singh, S. R. Dhakate, V. N. Singh and R. B. Mathur, *J. Mater. Chem. A*, 2013, **1**, 9138–9149.
23 P. Garg, B. P. Singh, G. Kumar, T. K. Gupta, I. Pandey, R. K. Seth, R. P. Tandon and R. B. Mathur, *J. Polym. Res.*, 2011, **18**, 1397–1407.
24 S. Pande, R. B. Mathur, B. P. Singh and T. L. Dhami, *Polym. Compos.*, 2009, **30**, 1312–1317.
25 T. K. Gupta, B. P. Singh, S. Teotia, V. Katyal, S. R. Dhakate and R. B. Mathur, *J. Polym. Res.*, 2013, **20**, 1–7.
26 B. P. Singh, Prabha, P. Saini, T. Gupta, P. Garg, G. Kumar, I. Pande, S. Pande, R. K. Seth, S. K. Dhawan and R. B. Mathur, *J. Nanopart. Res.*, 2011, **13**, 7065–7074.
27 B. P. Singh, D. Singh, R. B. Mathur and T. L. Dhami, *Nanoscale Res. Lett.*, 2008, **3**, 444–453.
28 W. Zhao, M. Fang, F. Wu, H. Wu, L. Wang and G. Chen, *J. Mater. Chem.*, 2010, **20**, 5817–5819.
29 R. Gupta, B. P. Singh, V. N. Singh, T. K. Gupta and R. B. Mathur, *Carbon*, 2014, **66**, 724–726.
30 G. Louarn, M. Cochet, S. Quillard, J. P. Buisson and S. Lefrant, *J. Raman Spectrosc.*, 2000, **31**, 1041–1049.
31 B. P. Singh, Prasanta, V. Choudhary, P. Saini, S. Pande, V. N. Singh and R. B. Mathur, *J. Nanopart. Res.*, 2013, **15**, 1–12.
32 B. P. Singh, P. Bharadwaj, V. Choudhary and R. B. Mathur, *Appl. Nanosci.*, 2013, 1–8.
33 R. Kumar, S. R. Dhakate, T. Gupta, P. Saini, B. P. Singh and R. B. Mathur, *J. Mater. Chem. A*, 2013, **1**, 5727–5735.
34 R. Kumar, S. R. Dhakate, P. Saini and R. B. Mathur, *RSC Adv.*, 2013, **3**, 4145–4151.
35 B. P. Singh, V. Choudhary, P. Saini and R. B. Mathur, *AIP Adv.*, 2012, **2**, 022151–022156.
36 T. Mäkelä, S. Pienimaa, T. Taka, S. Jussila and H. Isotalo, *Synth. Met.*, 1997, **85**, 1335–1336.
37 H. Zengin, W. Zhou, J. Jin, R. Czerw, D. W. Smith, L. Echegoyen, D. L. Carroll, S. H. Foulger and J. Ballato, *Adv. Mater.*, 2002, **14**, 1480–1483.
38 N. H. Hoang, J. L. Wojkiewicz, J. L. Miane and R. S. Biscarro, *Polym. Adv. Technol.*, 2007, **18**, 257–262.
39 S. W. Phang, M. Tadokoro, J. Watanabe and N. Kuramoto, *Curr. Appl. Phys.*, 2008, **8**, 391–394.
40 K. H. Wu, T. H. Ting, G. P. Wang, W. D. Ho and C. C. Shih, *Polym. Degrad. Stab.*, 2008, **93**, 483–488.
41 T.-H. Ting and K.-H. Wu, *J. Magn. Magn. Mater.*, 2010, **322**, 2160–2166.
42 L. Du, Y. Du, Y. Li, J. Wang, C. Wang, X. Wang, P. Xu and X. Han, *J. Phys. Chem. C*, 2010, **114**, 19600–19606.
43 H. Jianjun, D. Yuping, Z. Jia, J. Hui, L. Shunhua and L. Weiping, *Phys. B*, 2011, **406**, 1950–1955.
44 J. Yun, J. Im, H.-I. Kim and Y.-S. Lee, *Colloid Polym. Sci.*, 2011, **289**, 1749–1755.
45 Y.-J. Chen, N. D. Dung, Y.-A. Li, M.-C. Yip, W.-K. Hsu and N.-H. Tai, *Diamond Relat. Mater.*, 2011, **20**, 1183–1187.
46 P. Saini, V. Choudhary, B. P. Singh, R. B. Mathur and S. K. Dhawan, *Synth. Met.*, 2011, **161**, 1522–1526.
47 K. Chen, C. Xiang, L. Li, H. Qian, Q. Xiao and F. Xu, *J. Mater. Chem.*, 2012, **22**, 6449–6455.
48 H. Yu, T. Wang, B. Wen, M. Lu, Z. Xu, C. Zhu, Y. Chen, X. Xue, C. Sun and M. Cao, *J. Mater. Chem.*, 2012, **22**, 21679–21685.

49 M.-S. Cao, J. Yang, W.-L. Song, D.-Q. Zhang, B. Wen, H.-B. Jin, Z.-L. Hou and J. Yuan, *ACS Appl. Mater. Interfaces*, 2012, **4**, 6949–6956.
50 C. Basavaraja, W. Kim, D. Kim and D. Huh, *Colloid Polym. Sci.*, 2012, **290**, 829–838.
51 B. Belaabed, J. L. Wojkiewicz, S. Lamouri, N. El Kamchi and T. Lasri, *J. Alloys Compd.*, 2012, **527**, 137–144.
52 M. Faisal and S. Khasim, *Iran. Polym. J.*, 2013, **22**, 473–480.
53 S. Li, M. Gan, L. Ma, J. Yan, J. Tang, D. Fu, Z. Li and Y. Bai, *High Perform. Polym.*, 2013, DOI: 10.1177/0954008313487393.
54 N. E. Kamchi, B. Belaabed, J.-L. Wojkiewicz, S. Lamouri and T. Lasri, *J. Appl. Polym. Sci.*, 2013, **127**, 4426–4432.
55 P. Bhattacharya, S. Dhibar and C. K. Das, *Polym.-Plast. Technol. Eng.*, 2013, **52**, 892–899.